RASĀYAN *J. Chem.*
Vol. 19 | No. 4 | 2394-2404 | October-December | 2026
ISSN: 0974-1496 | e-ISSN: 0976-0083 | CODEN: RJCABP
http://www.rasayanjournal.com
http://www.rasayanjournal.co.in

RESISTIVE SWITCHING AND MEMORY CHARACTERISTICS OF MULTIFUNCTIONAL HETERO-MXENE COMPOSITE MEMRISTORS WITH WO_3 SWITCHING LAYER

S. Guvvala[1,✉] and S. M. Kalluru[2]
[1]Research Scholar, Department of Chemistry, Jawaharlal Nehru Technological University Anantapur, Andhra Pradesh, India
[2]Department of Chemistry, Jawaharlal Nehru Technological University Anantapur College of Engineering, Pulivendula, Andhra Pradesh, India
✉Corresponding author: sankarguvvala@gmail.com

ABSTRACT
The hetero-MXene ($Ti_3C_2T_x$/)/WO_3/ITO based multifunctional memristors were fabricated and investigated for nonvolatile memory applications. Various $Ti_3C_2T_x$/ based heterostructures (e.g., $Ti_3C_2T_x$/Activated Carbon, $Ti_3C_2T_x$//Lignin, $Ti_3C_2T_x$//MoS_2 and $Ti_3C_2T_x$//Graphene) were prepared via solution method and self-assembly. Synthesised hetero-MXenes were used as the conductive top electrode, and WO_3 was selected as the resistive switching layer with bottom electrode of ITO. Characterisations of structure and morphology confirmed the successful fabrication of a layered heterostructure with expanded interlayer spacing, porosity and effective interface coupling. Based on electrical characteristics, stable bipolar resistive switching with low operating voltage, endurance, ON/OFF ratio and retention has been achieved. Such improved performances come from a synergistic effect between MXene sheets and secondary functional materials to realise the mobility of oxygen vacancies and modulation of the the conductive filament inside WO_3. Heterostructures with graphene and MoS demonstrate better switching uniformity and retention memory compared with the other hetero-MXene heterostructures owing to the promotion of electronic conductivity and effective transport of carriers. This suggests that multifunctional hetero-MXene composite memristors could be a potential candidate for future neuromorphic and nonvolatile memories.
Keywords: Memristor, Hetero-MXene, WO_3, Resistive Switching, Non-Volatile Memory, $Ti_3C_2T_x$, Neuromorphic Computing.

RASĀYAN *J. Chem.*, Vol. 19, No.4, 2026

INTRODUCTION

Due to growing interest in high-speed, low-power, and scalable data storage systems, novel memory technologies are becoming subjects of great attention. Amongst various next-generation memories, resistive random access memory (RRAM) seems to be a promising candidate with its simple metal-insulator-metal structure, fast switching time, great scalability and good compatibility with neuromorphic circuits.[1] Resistive switching, that is, the reversibly tunable high and low resistance state (HRS/LRS), is based on conductive filament formation/rupture within an active switching layer.[2] Transition metal oxides such as TiO_2, ZnO, HfO_2, and WO_3 have been extensively researched as switching materials due to their good oxygen vacancy mobility and steady electrical behaviours.[3] Tungsten oxide (WO_3) gained significant attention for its broad band gap, good thermal stability, tunable conductivity and excellent defect-mediated switching behaviours.[4] The resistive switching properties in WO_3 are governed by mobile oxygen vacancies within the device and, under applied bias, create conducting pathways between the electrodes.[5] Recently, two-dimensional MXene materials, featuring metallic conductivity, large surface area, hydrophilic properties and controllable surface chemistry, have become more appealing materials for electronics and energy storage applications.[6] $Ti_3C_2T_x$ MXene shows particularly exciting potential in memristive devices owing to its excellent conductivity and tunable surface chemistry.[7] However, the electrical conductivity of pristine MXene layers is limited by the restacking phenomenon, lack of mobile ion access, etc.[8] To solve this issue, hetero-MXenes incorporated with activated carbon, lignin, MoS_2, and graphene are developed to enhance the electrical conductivity, ion diffusion, surface area, and interfacial coupling.[9] The synergistic effect between different constituent layers results in expanded interlayer

http://doi.org/10.31788/RJC.2026.1949997
This work is licensed under a CC BY 4.0 license.

spacing, good carrier transport, porous structures and active sites.[10] This kind of composite nature is beneficial for the stability and reliability of conductive filaments within memristive systems. The multifunctional Hetero-MXene memristor based on a Hetero-MXene/WO_3/ITO heterostructure is fabricated and studied in this work. $Ti_3C_2T_x$-based Hetero-MXenes are selected as top electrodes for investigating their effect on the resistive switching and memory characteristics. The electrical performances of different Hetero-MXenes are systematically studied and analysed.

Material Synthesis and Device Fabrication

Synthesis of Delaminated $Ti_3C_2T_x$ MXene

$Ti_3C_2T_x$ MXene was prepared by the wet chemical etching method of the Ti_3AlC_2 MAX phase. Aluminium interlayers of the MAX phase were removed by selective etching using a mixed solution of HCl and HF.1:1 The precipitated multilayer MXene was washed and centrifuged many times until neutral pH was reached. The delaminated $Ti_3C_2T_x$ nanosheets were obtained through intercalation of LiCl, resulting in improved exfoliation and colloidal stability.[12]

The etching reaction is expressed as:

$$Ti_3AlC_2 + HF \rightarrow Ti_3C_2T_x + AlF_3 + H_2$$

Where T_x represents surface terminations such as –OH, –O, and –F.

Preparation of Hetero-MXene Composites

$Ti_3C_2T_x$/Activated Carbon Hetero-MXene

The above d-$Ti_3C_2T_x$ was added Activated Carbon 1:1 ratio. These composites were then subjected to ultrasonication for 6 hours to produce colloidal suspensions of activated carbon-integrated MXene composite mixture. Afterwards, these solutions was individually mixed via a magnetic stirrer for 30 min, followed by an ultrasonication treatment (duration: 30 min). Furthermore, the obtained colloidal solution.[13]

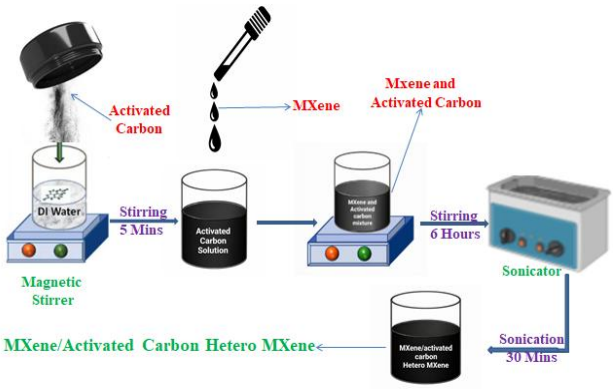


Fig.-1: Schematic Illustration of the Synthesis Process for the MXene/Activated Carbon Hetero MXene Composite via Sequential Magnetic Stirring and Ultrasonication

$Ti_3C_2T_x$/Lignin Hetero-MXene

In a reaction bottle, 1 gm of lignin was added, then 10 ml 0.1M NaOH solution was added and stirred on a magnetic stirrer for 2 hours.[12,13] Lignin was dissolved; a homogeneous dark brown solution formed. The lignin solution was added slowly dropwise into the prepared d- $Ti_3C_2T_x$ MXene solution and mixed for 6 hours after 30 min sonication to obtain a colloidal $Ti_3C_2T_x$ /Lignin hetero MXene solution.[14]

$Ti_3C_2T_x$/MoS_2 Hetero-MXene

The heterostructure composite was synthesized by the one-step mixing and self-assembling strategy. A given amount of $Ti_3C_2T_x$ dispersion was added to the MoS_2 nanosheets solution with a designated weight ratio of 1:1.[20,21] The mixed solution was stirred for 8 hours to guarantee homogeneous contact between them and then was mildly ultrasonicated for 30 min to increase interface connection. Finally, the product $Ti_3C_2T_x$/MoS_2 composite hetero MXene solution was collected via centrifugation.[15]

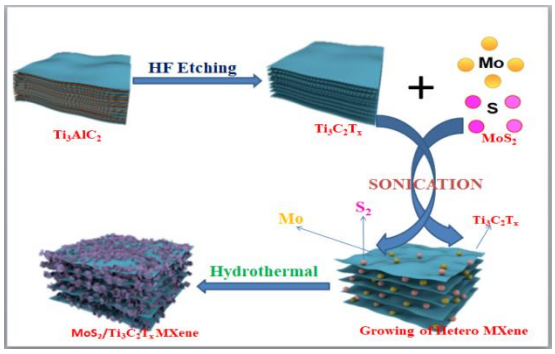


Fig.-2: Schematic Illustration of the Synthesis Protocol for the $MoS_2/Ti_3C_2T_x$ MXene Hetero Structure. The Process Involves The Selective HF Etching of the Ti_3AlC_2 MAX Phase, Followed by the Incorporation of Mo and S Precursors Through Sonication and Subsequent Hydrothermal Growth of MoS_2 Nanostructures on the MXene Templates

$Ti_3C_2T_x$/Graphene Hetero-MXene

The fabrication of $Ti_3C_2T_x$/graphene hetero-composite is through a straightforward solution-based self-assembly technique. The 2-D materials can be incorporated without complex processing steps, where a well-dispersed colloidal solution of $Ti_3C_2T_x$ MXene nanosheets is prepared and mixed with a graphene-based solution (eg: graphene oxide (GO)) in a controlled ratio of 1:1, which may provide a suitable interface and can control the properties of the final composite.[28,29] This mixture is sonicated for about 60 mins to break the agglomeration of the nanosheets and achieve uniform dispersion of $Ti_3C_2T_x$ and graphene throughout the mixture. The ultrasonic waves help to establish a strong interlinking at the interfaces between $Ti_3C_2T_x$ and graphene layers, resulting in a homogeneous composite structure.[30] The mixture is then allowed to stir for 6 hours at room temperature for self-assembly. Self-assembly of the hetero-structure of $Ti_3C_2T_x$ /graphene occurs spontaneously due to the electrostatic attractive forces and van der Waals force interactions between the negatively charged functional groups (-OH, -O, -F) present on the surface of MXene layers and the graphene sheets. Such type of process can contribute to efficient charge transport in the material, especially at the interfaces, improving the performance in terms of electrical characteristics and hence making them ideal candidates for use in photodetectors, sensors, energy storage, etc.[31]

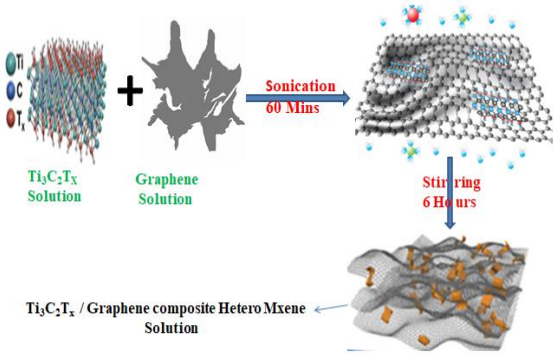


Fig.-3: Schematic Representation of the Fabrication of $Ti_3C_2T_x$/Graphene Hetero-MXene Composite, where $Ti_3C_2T_x$ Nanosheets and Graphene Dispersion are Combined Through Solution Mixing, Followed by Ultrasonication to Enhance Dispersion and Stirring to Promote Interfacial Interaction and Heterostructure Formation

Memristor Fabrication

ITO-coated glass substrates were cleaned sonically in acetone, ethanol, and deionised water. WO_3 switching layer was spin-coated on the ITO substrate and thermally annealed. Finally, synthesised hetero-MXene composites were drop-cast as the top electrode and then vacuum-dried. The final device structure is represented as: Hetero-MXene / WO_3 / ITO.

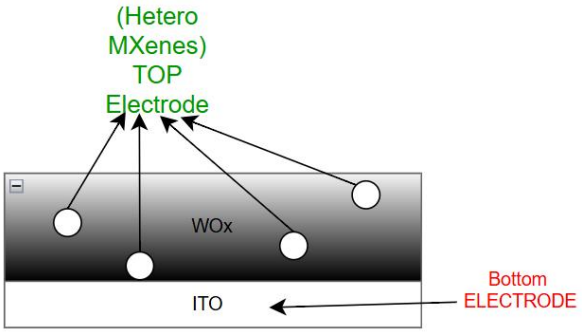


Fig.-4: Schematic Illustration of Fabrication of Device Structure

Structural and Morphological Analysis

To examine the structural and morphological properties of synthesised hetero-MXene composites and to identify how they can affect the resistive switching characteristics of the fabricated memristor devices, the samples were subjected to analysis using X-ray diffraction (XRD), scanning electron microscopy (SEM), and transmission electron microscopy (TEM). The collected data confirm the formation of layered, multifunctional hetero-MXene structures that possess increased interfacial interaction, increased interlayer distance and a better conductive path. The XRD patterns indicate the formation of $Ti_3C_2T_x$ MXene and its heterostructures with AC, Lig, MS, and Gr. The XRD pattern for the undiluted $Ti_3C_2T_x$ MXene exhibits a characteristic diffraction peak centred around 2 = 9, associated with the (002) plane of the 2D layered $Ti_3C_2T_x$ structure obtained by delaminating the Ti_3AlC_2 MAX phase using selective etching.[17] Shifting of this peak to the smaller diffraction angle indicates the delamination of Al layers, and the appearance of terminal groups like-OH, -O, and -F between MXene layers expand interlayer space. For the hetero-MXene composites, while the MXene diffraction peaks appear, a slight shift to a lower angle with decreasing intensity proves that the second materials are intercalated between MXene layers and strong interfacial coupling is generated.[18] Broad diffraction features are associated with the AC/Lig, as they are not well-crystalline structures, while the crystal diffraction peaks belonging to MoS_2 are seen to grow on MoS_2/MXene composites. The graphitic carbon diffraction peak can be identified around 2 = 25 in Gr/MXene composites, confirming that the hybrid structure is formed. The improved charge transport across the layer is due to enhanced electron mobility and ion transport, as the expanded interlayer distance allows rapid migration of electrons. SEM analysis provided insight into the surface morphologies of the materials synthesised. The undiluted $Ti_3C_2T_x$ MXene shows the typical accordion-like stacked layer, which is formed during the exfoliation process of the MAX structure.[20] After heterostructure formation, different morphological features are found. A porous and interconnected networked morphology with a rough surface is found on AC/MXene composite due to the uniform dispersal of AC particles within the MXene sheets, enhancing electron transport. In Lig/MXene composites, strong hydrogen bonding and electrostatic interaction causes more compact layered morphology with enhanced interfacial contact.[21] MoS_2 nanosheets grow on the MXene layers in MoS_2/MXene composites in a stacked wrinkled structure with abundant active sites, and in the case of Gr/MXene composites, a highly crumpled and overlapped layered structure formed efficiently facilitates charge transport.[22] No macroscopic aggregates are found to form, indicating the uniformity of the synthesised heterostructures. TEM analysis further verifies the successful formation of layered hetero-MXene composites. Ultra-thin transparent MXene sheets are identified, clearly showing their well-defined layered structures, proving the effective exfoliation of the $Ti_3C_2T_x$ MAX structure.[23] The activated carbon, lignin, MoS_2, and graphene layers can be observed on the surface or within the layers of the $Ti_3C_2T_x$ MXene structure, and there are strong interactions between layered materials.[24] Clearly visible lattice fringes from selected area electron diffraction analysis confirmed the crystal lattice formed after heterostructure construction. The presence of semi-crystalline diffraction rings shown in SAED patterns of different materials indicates the formation of heterostructures. Overall, all of the structural and morphological analyses exhibit increased interlayer spacing, increased porosity, and enhanced interfacial coupling, which is desirable for electron transport, conductive filament stability, and efficient oxygen

vacancies migration in the WO_3 layer to obtain excellent endurance and stability of the constructed Hetero-MXene/WO_3/ITO memristor device.

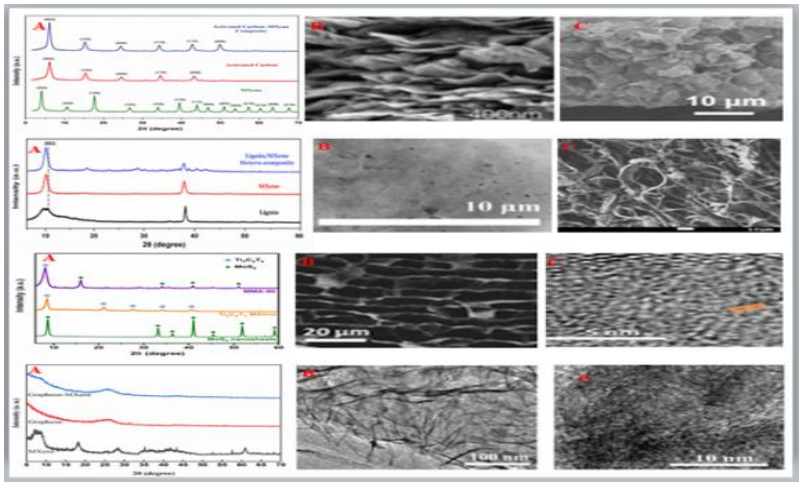


Fig.-5: Schematic Representation of the Fabrication of Hetero-MXene Characterisations: (A) XRD Analysis of all Hetero MXenes (B) TEM Analysis of all Hetero MXenes (C) SEM Analysis of all Hetero MXenes

Electrical Characterization

The electrical properties of the fabricated Hetero-MXene/WO_3/ITO memristor devices were characterised using I-V measurements, endurance cycling, retention tests, and conduction mechanism. From the measurements, it was confirmed that the hetero-MXene/WO_3/ITO devices have reliable bipolar resistive switching characteristics with good memory stability, low operating voltage, and switchable cyclability. The functional hetero-MXene top electrode largely improves the charge mobility, steady conductive filaments, and stable switching behaviour of theWO_3 switching layer. Based on the electrical characteristic testing results, these fabricated devices can potentially be used in non-volatile memory and neuromorphic computation applications.

Current–Voltage (I–V) Characteristics

Figure-6 shows the measured I-V characteristics. Our memristor device showed the resistive switching properties under the cyclic DC voltage sweep operation. The sweeping range of voltage was 0 V to +3 V, and current was measured with hetereo-MXene as the top electrode and ITO as the bottom electrode with grounded potential. Our device was initialised to a High Resistance State (HRS) and showed minimal leakage current in the initial state. When we applied voltage from 0V to positive with a step voltage of 0.1V, the current increased gradually with applied voltage. When the applied voltage was approximately +1.8V sudden current surge occurred, which corresponds to the SET process, and the device changed to a Low Resistance State (LRS). As we increased the SET current from 10^{-6} A to approximately 10^3A, the conductive filaments formation in theWO_3 Switching Layer was formed. Conductive filament forms with oxygen ions moving far from their original lattice sites when applying electric field is applied. An oxygen vacancy is created behind the removed oxygen ion. Oxygen vacancies accumulate to form a conducting path between the hetero-MXene electrode and the bottom electrode of ITO.[25] Because of enhanced carrier injection and even electric field distribution of hetero-MXene, conductive filaments are more easily formed. While the applied voltage decreased from 0V to negative, until the the applied voltage was about -1.5V device remained in the LRS. A sudden drop in current occurred, which was interpreted as the RESET process. It recovered from LRS to HRS with rupture of the conductive filament caused by the combination of oxygen ions with oxygen vacancies.[26] The obtained I-V curve clearly showed hysteresis loops and clearly showed bipolar resistive switching behaviour. Our device shows good, reproducible and stable switching cycles, and the on/off resistance ratio is about 10^3–10^4. This resistance ratio is considered good enough for secure data storage applications. Between all of the fabricated devices, Graphene/ MXene and MoS/ MXene heterostructures had a smaller SET voltage and smoother switching characteristics because of higher conductivity and better electron transport at the interface.

Endurance Characteristics

For demonstrate the endurance characteristics of the memristor device, the device was repeatedly switched between HRS and LRS states by applying consecutive SET and RESET voltage pulses and read out its resistance value by applying a read voltage of 0.1 V for every switching cycle. Endurance characteristics are shown in Fig.-6.

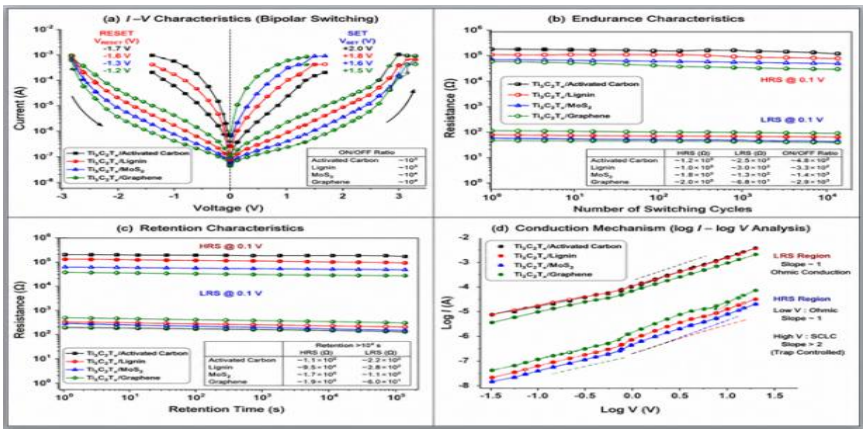


Fig.-6: Schematic Representation of the Fabrication of Hetero MXene Electrochemical Characterisation All Fabricated Devices (a) I-V Characteristics (b) Endurance Characteristics (c) Retention Characteristics (d) Conduction Mechanism

In Section four, The device shows reliable resistive switching for over 10^3 repeated switching cycles without significant degradation. The high-resistance state is roughly ~10^5 Ω , while the low-resistance state is roughly ~10^2Ω . The good switching characteristics are confirmed by well-definedHRS andLRS states separated by a high resistance ratio and good repeatability. The small fluctuations in resistance value suggest stable formation/rupture of filamentary paths during repeated operations.[27] The great endurance is due to the fact that hetero-MXene and WO_3 display a strong interaction interface, limited oxygen vacancies and suppressed filament instability, good transport characteristics of carriers, etc. The outstanding endurance of the graphene/MXene heterostructure comes from the excellent conduction property of graphene, which reduces local heating at the filament during switching.

Retention Characteristics

To test the stability of the long-term non-volatile memory, we measured the retention performance. The resistances in the two different states are recorded at room temperature without read operation over time (read voltage is kept at 0.1V constantly). The retention curve is shown in Fig.-4. As it is shown, the device can keep both states stable without degradation over 10^4 seconds. The HRS state value is maintained nearly constant around 10^5 seconds, while the LRS state value is maintained at around 10^2 Ω during the retention measurements.[28] The stable maintenance of the memory characteristics shows that the formed conductive filaments in the WO switching layer are strong and would not collapse under the common conditions. With a hetero-MXene electrode structure, the charge transport ability can be improved, and the oxygen vacancy distribution in the switching layer is more stable. Because of the structure of layered structure of hetero-MXene composites, charge trapping could be reduced, and the current leakage is also eliminated.

Conduction Mechanism Analysis

The conduction mechanism of the memristor device was analysed using log(I)–log(V) plots derived from the I–V characteristics, as shown in Fig.6. Section four. Two separate conduction areas corresponding to HRS and LRS states are demonstrated by the analysis. When the device was in the low resistance state, the slope of the log(I)–log(V) curve approached 1, which is characteristic of ohmic conduction. This confirms that continuous conductive filaments formed by oxygen vacancies dominate current transport.[29] Nonlinear current behaviour was detected when the system was in a high-resistance state. At low voltages, current increased linearly because of thermally generated free carriers. The slope rose substantially at

elevated voltages as a result of trap-controlled space-charge-limited conduction (SCLC).[30] The WO_3 layer contains oxygen vacancy defect states that trap injected carriers in this region. The resistive switching process is therefore controlled by oxygen vacancy generation, conductive filament formation, filament rupture, carrier trapping and de-trapping.

Performance Comparison And Switching Mechanism

The synthesised Hetero-MXene/WO_3/ITO memristor devices showed superior resistive switching properties compared to conventional WO-based memristors. The introduction of the hetero-MXene composite electrode, such as $Ti_3C_2T_x$/Activated Carbon, $Ti_3C_2T_x$/Lignin, $Ti_3C_2T_x/MoS_2$, and $Ti_3C_2T_x$/Graphene, not only improved the electrical conductivity, interfacial charge transport, oxygen vacancy migration and conductive filament stability, but also brought out lower switching voltage, better endurance properties, and outstanding ON/OFF resistance ratio and retention performance. Among all the manufactured devices, the $Ti_3C_2T_x$/Graphene hetero-MXene memristor delivered excellent switching characteristics with the help of a highly conductive graphene layer for rapid charge carrier transport and less charge carrier recombination. Its SET voltage is as low as about 1.5 V, and its RESET voltage remains stable around -1.2 V, whereas its ON/OFF resistance ratio is as high as about 10^4 s. The high conductivity of the graphenes improves electric field distribution uniformity for the WO_3 switching layer, thus creating a stable conductive filament and weakening the fluctuation.[32] The $Ti_3C_2T_x/MoS_2$ heterostructure presented excellent switching uniformity and outstanding retention properties. Its layered MoS_2 nanosheets provide abundant catalytic sites, enhance interactions with MXene sheets, which promote the accumulation of oxygen vacancies, as well as inhibit the accidental rupture of conductive filaments.[33] The resistance state of the device was kept unchanged after more than 10^4 s. For the $Ti_3C_2T_x$/Activated Carbon composite device, activated carbon is composed of a highly porous structure, which expands the pathways of ion transport. It benefits oxygen ion migration and the formation of conductive filaments due to the porous design for the WO switching layer.[34] The device presents good endurance and reliable bipolar switching, though the switching voltage is a bit higher than that of graphene/MXene devices. For the $Ti_3C_2T_x$/Lignin structure, it presents stable resistive switching and good flexibility and environmental friendliness properties owing to strong hydrogen bond interaction between lignin molecules and MXene nanosheets.[35] But compared to graphene and MoS_2-based heterostructures, the conductivity of the lignin composite material is lower, resulting in a higher switching voltage and less current passing through the device. The switching behaviour of the prepared memristor devices is mainly attributed to the migration of oxygen vacancies and formation of the conductive filament in theWO_3 switching layer. Under the application of a positive voltage on the hetero-MXene top electrode, the oxygen ions move out from the lattice site to create oxygen vacancies. Gradually increasing numbers of oxygen vacancies are produced to form the conductive filament, which bridges between the top hetero-MXene electrode and bottom ITO electrode, thus devices switch from the High Resistance State (HRS) to the Low Resistance State (LRS).[36]

The conductive filament formation process can be represented as:

$$WO_3 \xrightarrow{Electric\ Field} WO_{3-x} + xV_O^{\bullet\bullet} + xe^-$$

Where $V_O^{\bullet\bullet}$ represents oxygen vacancies generated inside the WO_3 layer.

An applied reverse voltage leads to the oxygen ions moving with oxygen vacancies, resulting in breakdown of conductive filaments and high resistive-state recovery of the materials. In other words, reversible forming and breaking of filaments results the bipolar resistive switching behaviour.[37] Multi-component hetero-MXene layers effectively guarantee better switching reliability through the following methods: boosted electric conductivity, expanded contact area, homogenising electric field distribution, regulating migration of oxygen vacancies and minimising arbitrary filament instability. The porous layered structures identified through structural study are beneficial for speedy ion diffusion and charge carrier transport, which leads to reduced power consumption and improved switching speed. As a result, the combination of MXene and the co-functional materials plays a crucial role in boosting the total memory performance of the produced devices. It can be seen from the obtained result, multifunction

hetero-MXene composite memristors provide promising applications in novel non-volatile memory, artificial synapses and neural networks, as well as flexible electronics in future.

Applications of Hetero-MxenE/WO_3/ITO Memristor Devices

The fabricated, multifunctional, Hetero-MXene/WO_3/ITO memristor devices possess good resistive switching behaviour, low switching voltage, high ON/OFF resistance ratio, stable endurance, and long retention stability, enabling their optimal utilisation in diverse emerging electronics and memory technologies. Electrical conductivity, ionic transport, and conductive filament stability are enhanced through the interplay of hetero-MXene electrodes and the WO_3 switching layer for high performance and energy efficiency. These Hetero-MXene/WO_3/ITO memristor devices hold significant promise for non-volatile memory storage, addressing the drawbacks of traditional memory systems in terms of energy consumption, scalability, and speed by utilising bistable resistive switching between high and low resistance states. The large ON/OFF resistance ratio (~10^5-10^2) facilitates the reliable differentiation of binary states, ideal for high-density resistive random-access memory (RRAM). The device also shows great potential for neuromorphic computing systems, mirroring the learning and memory capabilities of biological synapses with gradual resistive switching for synaptic weight modulation. The consistent conductive filament formation and ion migration in the WO_3 layer promote analogue switching characteristics suitable for artificial neural networks and brain-inspired computing. The improved electrical conductivity and carrier mobility of $Ti_3C_2T_x$/Graphene and $Ti_3C_2T_x$ /MoS_2 heterostructures further make them ideal for energy-efficient neuromorphic applications. The consistent endurance and retention characteristics enable repetitive learning cycles. The low switching voltage (approximately 1.5-1.8 V) is also beneficial for power efficiency in synaptic operation. The Hetero-MXene memristors also excel in flexible and wearable electronics due to their superior mechanical flexibility, light weight, and high surface conductivity, making them ideal for flexible memory devices, wearable sensors, and intelligent electronics. These devices can also be utilised in AI hardware accelerators and in-memory computing systems, circumventing the data transfer bottlenecks of traditional computing architectures by enabling both data storage and computation within a single device, perfect for efficient parallel information processing. Furthermore, their large surface area and improved ion transport capabilities make them excellent for sensing applications like gas and photodetectors, as well as for adaptive electronics and the detection of environmental stimuli, due to a well-formed conductive network with MXene heterostructures and improved sensitivity and stability. The environmentally friendly, solution-based synthesis process for the created hetero-MXene materials also allows for scalable and cost-effective device fabrication, while lignin-based heterostructures offer biodegradability and sustainability. In summary, the Hetero-MXene/WO_3/ITO memristor devices demonstrate exceptional performance and multifaceted capabilities for non-volatile memory, neuromorphic computing, artificial synapses, flexible electronics, wearable systems, AI accelerators, in-memory computing, and sensing applications. Their enhanced electrical performance and multifunctional characteristics underscore their strong potential in the fields of nanoelectronics and brain-inspired computing.

CONCLUSION

This study presented the fabricated and characterised multifunctional heterogeneous MXene/WO_3/ITO memristor device to explore its potential for resistance switching applications and as a nonvolatile memory device. Various $Ti_3C_2T_x$-based heterogeneous MXene composites: $Ti_3C_2T_x$/Activated Carbon, $Ti_3C_2T_x$/Lignin, $Ti_3C_2T_x$/MoS_2, and $Ti_3C_2T_x$/Graphene was synthesised via solution-based self-assembly and ultrasonication methods. These hetero-structured composites were used as the top electrodes; tungsten oxide (WO_3) was used as the active switching layer, and indium tin oxide (ITO) was used as the bottom electrode. Structural and morphological studies by XRD, SEM, and TEM revealed that layer-structured heterogeneous MXene composites with a large interlayer gap and porous nature are formed, with effective interfacial interaction between MXene and other functional materials. The large layered space and porous composite provide increased electron transport ability and better oxygen ion migration within the WO_3 layer to facilitate the resistive switching. Electrical characteristics of these hetero structure composite memristor revealed stable bipolar resistive switching behaviour with low set and reset

switching voltages, a large ON/OFF ratio (>10 ^{4}) and a long retention time (> 10^4 s), good endurance performance over 100 cycles and also efficient nonvolatile memory application. It was observed that the switching mechanism is mainly controlled by oxygen vacancy migration and reversible formation and destruction of the conductive filament within the WO_3 layer. Using hetero-MXene as an electrode helps the device show enhanced conductive filament stability and uniform electric-field distribution. Also, hetero-MXene effectively promoted electron transport at the interface and hence improved switching reproducibility and lower power consumption. Among all four devices studied, $Ti_3C_2T_x$-/Graphene and $Ti_3C_2T_x$-/MoS_2devices provided excellent nonvolatile memory properties due to the excellent electrical conductivity, effective carrier transport channel and the good interfacial binding energy of the compounds. Activated carbon-based materials endow better porous properties and more ionic diffusion to the devices, while lignin-based devices provided eco-friendly and stable memory properties. The promising results indicated that these multi-functional heterogeneous MXene composite memristors would have great potential for non-volatile memories, artificial neural networks, artificial synaptic devices, and flexible and smart nanoelectronic devices in the future, with simple and low-cost solution process and outstanding electronic performance and multi-functional characteristics.

ACKNOWLEDGEMENTS

The authors gratefully acknowledge IIT Hyderabad for providing the necessary research facilities and financial support to carry out this study under the ANRF–PAIR programme. The authors also express their sincere thanks to Dr. Narendra Kurra and Dr. Suresh Kumar Garlapati for their valuable guidance, encouragement, and continuous support of this work.

CONFLICT OF INTERESTS

The authors declare that they have no conflicts of interest regarding the publication of this manuscript.

AUTHOR CONTRIBUTIONS

The present work is related to *SDG-9: Industry, Innovation and Infrastructure*. All the authors contributed significantly to this manuscript, participated in reviewing/editing and approved the final draft for publication. The research profile of the authors can be verified from their ORCID ids, given below:

S. Guvvala https://orcid.org/0009-0000-8050-4644
S. M. Kalluru https://orcid.org/0000-0003-4249-8241

Open Access: This article is distributed under the terms of the Creative Commons Attribution 4.0 International License (http://creativecommons.org/licenses/by/4.0/), which permits unrestricted use, distribution, and reproduction in any medium, provided you give appropriate credit to the original author(s) and the source, provide a link to the Creative Commons license, and indicate if changes were made.
Cite this article as: S. Guvvala and S. M. Kalluru, *Rasayan J. Chem.*, 19(4), 2394-2404(2026), https://doi.org/10.31788/RJC.2026.1949997

REFERENCES

1. L. O. Chua, *IEEE Transactions on Circuit Theory*, **18**, 507(1971), https://doi.org/10.1109/TCT.1971.1083337.
2. D. B. Strukov, G. S. Snider, D. R. Stewart and R. S. Williams, *Nature*, **453**, 80(2008),https://doi.org/10.1038/nature06932.
3. R. Waser and M. Aono, *Nature Materials*, **6**, 833(2007), https://doi.org/10.1038/nmat2023.
4. R. Waser, R. Dittmann, G. Staikov and K. Szot, *Advanced Materials*, **21**, 2632(2009),https://doi.org/10.1002/adma.200900375.
5. D. Ielmini, *IEEE Transactions on Electron Devices*, **58**, 4309(2011),https://doi.org/10.1109/TED.2011.2167513.
6. D. Ielmini and H.-S. P. Wong, *Nature Electronics*, **1**, 333(2018), https://doi.org/10.1038/s41928-018-0092-2.
7. H.-S. P. Wong, H. Y. Lee, S. Yu, Y. S. Chen, Y. Wu, P. S. Chen, B. Lee, F. T. Chen and M. J. Tsai, *Proceedings of the IEEE*, **100**, 1951(2012), https://doi.org/10.1109/JPROC.2012.2190369.

8. S. Yu, *Proceedings of the IEEE*, **106**, 260(2018), https://doi.org/10.1109/JPROC.2018.2797526.
9. J. J. Yang, D. B. Strukov and D. R. Stewart, *Nature Nanotechnology*, **8**, 13(2013), https://doi.org/10.1038/nnano.2012.240.
10. J. J. Yang, M. D. Pickett, X. Li, D. A. A. Ohlberg, D. R. Stewart and R. S. Williams, *Nature Nanotechnology*, **3**, 429(2008), https://doi.org/10.1038/nnano.2008.160.
11. S. Jo, K.-H. Kim, K. Narayanan, B. Lu and H. Hwang, *Nano Letters*, **10**, 1297(2010),https://doi.org/10.1021/nl904092h.
12. M. Prezioso, F. Merrikh-Bayat, B. D. Hoskins, G. C. Adam, K. K. Likharev and D. B. Strukov, *Nature*, **521**, 61(2015), https://doi.org/10.1038/nature14441.
13. S. Kwon, J. H. Park, J. H. Lee, S. Kim and K. Kim, *Nature Nanotechnology*, **5**, 148(2010),https://doi.org/10.1038/nnano.2009.456.
14. D. B. Strukov and H. Kohlstedt, *MRS Bulletin*, **37**, 108(2012), https://doi.org/10.1557/mrs.2012.2.
15. M. Naguib, M. Kurtoglu, V. Presser, J. Lu, J. Niu, M. Heon, L. Hultman, Y. Gogotsi and M. W. Barsoum, *Advanced Materials*, **23**, 4248(2011), https://doi.org/10.1002/adma.201102306.
16. M. Ghidiu, M. R. Lukatskaya, M.-Q. Zhao, Y. Gogotsi and M. W. Barsoum, *Nature*, **516**, 78(2014), https://doi.org/10.1038/nature13970.
17. M. Alhabeb, K. Maleski, B. Anasori, P. Lelyukh, L. Clark, S. Sin and Y. Gogotsi, *Chemistry of Materials*, **29**, 7633(2017), https://doi.org/10.1021/acs.chemmater.7b02847.
18. Y. Gogotsi and B. Anasori, *ACS Nano*, **13**, 8491(2019), https://doi.org/10.1021/acsnano.9b06394.
19. B. Anasori, M. R. Lukatskaya and Y. Gogotsi, *Nature Reviews Materials*, **2**, 16098(2017),https://doi.org/10.1038/natrevmats.2016.98.
20. M. R. Lukatskaya, O. Mashtalir, C. E. Ren, Y. Dall'Agnese, P. Rozier, P. L. Taberna, M. Naguib, P. Simon, M. W. Barsoum and Y. Gogotsi, *Science*, **341**, 1502(2013), https://doi.org/10.1126/science.1241488.
21. A. Shahzad, B. S. E. H. Anasori, M. R. Lukatskaya, Y. Gogotsi and M. W. Barsoum, *Science*, **353**, 1137(2016), https://doi.org/10.1126/science.aag2421.
22. L. Verger, V. Natu, M. Carey and M. W. Barsoum, *Trends in Chemistry*, **1**, 656(2019),https://doi.org/10.1016/j.trechm.2019.04.006.
23. M. Shekhirev, C. E. Shuck, A. Sarycheva and Y. Gogotsi, *Progress in Materials Science*, **120**, 100757(2021), https://doi.org/10.1016/j.pmatsci.2020.100757.
24. M. Downes, C. E. Shuck, B. McBride et al., *Nature Protocols*, **19**, 1807(2024), https://doi.org/10.1038/s41596-024-00969-1.
25. C. E. Shuck, M. Han, K. Maleski et al., *ACS Chemical Health & Safety*, **28**, 326(2021),https://doi.org/10.1021/acs.chas.1c00051.
26. Y.-J. Kim, S. J. Kim, D. Seo, Y. Chae, M. Anayee, Y. Lee, Y. Gogotsi, C.-W. Ahn and H.-T. Jung, *Chemistry of Materials*, **33**, 6346(2021), https://doi.org/10.1021/acs.chemmater.1c01263.
27. X. Wang, C. Garnero, G. Rochard, D. Magne, S. Morisset, S. Hurand, P. Chartier, J. Rousseau, T. Cabioc'h and C. Coutanceau, *Journal of Materials Chemistry A*, **5**, 22012(2017),https://doi.org/10.1039/C7TA01082F.
28. M.-Q. Zhao, N. Trainor, C. E. Ren, M. Torelli, B. Anasori and Y. Gogotsi, *Advanced Materials Technologies*, **4**, 1800639(2019),https://doi.org/10.1002/admt.201800639.
29. J. Zhang et al., *Advanced Materials*, **32**, 2001093(2020), https://doi.org/10.1002/adma.202001093.
30. M. Naguib, J. Halim, J. Lu, K. M. Cook, L. Hultman, Y. Gogotsi and M. W. Barsoum, *Journal of the American Chemical Society*, **135**, 15966(2013), https://doi.org/10.1021/ja405735d.
31. X. Yan, K. Wang, J. Zhao, Z. Zhou, H. Wang, J. Wang, L. Zhang, X. Li, Z. Xiao, Q. Zhao, Y. Pei, G. Wang, C. Qin, H. Li, J. Lou, Q. Liu and P. Zhou, *Small*, **15**, e1900107(2019), https://doi.org/10.1002/smll.201900107.
32. C. Choi et al., *Advanced Electronic Materials,* **7(2)**, 2000866(2021), https://doi.org/10.1002/aelm.202000866.
33. A. C. Khot, T. D. Dongale, J. H. Park, A. V. Kesavan and T. G. Kim, *ACS Applied Materials & Interfaces*, **13**, 5216(2021), https://doi.org/10.1021/acsami.0c19028.

34. X. Feng, J. Huang, J. Ning, D. Wang, J. Zhang and Y. Hao, *Carbon*, **205**, 365(2023),https://doi.org/10.1016/j.carbon.2023.01.040.
35. B. Jana and A. Roy Chaudhuri,*Chips*, **3**, 235(2024), https://doi.org/10.3390/chips3030012.
36. Y.-T. Li, S.-B. Long, H.-B. Lü, Q. Liu, Q. Wang, Y. Wang, S. Zhang, W.-T. Lian, S. Liu and M. Liu, *Chinese Physics B*, **20**, 017305(2011), https://doi.org/10.1088/1674-1056/20/1/017305.
37. S. Lee, K. H. Yun and D. Kim, *Thin Solid Films*, **674**, 91(2019),https://doi.org/10.1016/j.tsf.2019.02.012.
38. J. Kim, A. I. Inamdar, Y. Jo, H. Woo, S. Cho, S. M. Pawar, H. Kim and H. Im, *ACS Applied Materials & Interfaces*, **8**, 9499(2016), https://doi.org/10.1021/acsami.5b11781.
39. S. Lamichhane, S. Sharma, M. Tomar and A. Chowdhuri, *Journal of Applied Physics*, **132**, 134102(2022), https://doi.org/10.1063/5.0103236.
40. K. Hadiyal, N. Raghavan and R. M. Thamankar, *Advanced Electronic Materials*, **12**, e00658(2026), https://doi.org/10.1002/aelm.202500658.
41. K. S. Novoselov, A. K. Geim, S. V. Morozov, D. Jiang, Y. Zhang, S. V. Dubonos, I. V. Grigorieva and A. A. Firsov, *Science*, **306**, 666(2004), https://doi.org/10.1126/science.1102896.
42. K. F. Mak, C. Lee, J. Hone, J. Shan and T. F. Heinz, *Physical Review Letters*, **105**, 136805(2010), https://doi.org/10.1103/PhysRevLett.105.136805.
43. B. Radisavljevic, A. Radenovic, J. Brivio, V. Giacometti and A. Kis, *Nature Nanotechnology*, **6**, 147(2011), https://doi.org/10.1038/nnano.2010.279.
44. F. H. L. Koppens, T. Mueller, P. Avouris, A. C. Ferrari, M. S. Vitiello and M. Polini, *Nature Nanotechnology*, **9**, 780(2014), https://doi.org/10.1038/nnano.2014.215

[RJC-9997/2026]